C. R. Chimie 16 (2013) 704–711

Contents lists available at SciVerse ScienceDirect

Comptes Rendus Chimie

www.sciencedirect.com

Full paper/Mémoire

Structural characterization and activation energy of $NiTiO_3$ nanopowders prepared by the co-precipitation and impregnation with calcinations

Mohamed Abd El-Fattah Gabal *, Yasser Mohamed Al Angari, Abdallah Yousef Obaid

Chemistry department, Faculty of Science, King Abdulaziz University, Jeddah, Saudi Arabia

ARTICLE INFO

Article history:
Received 19 November 2012
Accepted after revision 16 January 2013
Available online 7 March 2013

Keywords:
$NiTiO_3$
XRD patterns
BET
Kinetic
Activation energy

ABSTRACT

In this paper, we report on the formation of novel hexagonal $NiTiO_3$ nanopowders synthesized by the impregnation or co-precipitation methods through the thermal decomposition reaction of the precursors. The decomposition course was followed using differential thermal analysis (DTA) and thermogravimetric analysis (TGA) techniques. The intermediate decomposition products as well as the formed titanate were characterized using X-ray diffraction (XRD) and Fourier transform infrared (FT-IR) spectroscopy. XRD patterns of the precursors calcined at 1000 °C showed the formation of the single ilmenite-type rhombohedral structure only with the impregnated precursor, while with the precipitated $NiTiO_3$ powders one it indicates the presence of some NiO and TiO_2 impurities. Transmission electron microscopy (TEM) exhibited loosely agglomerated hexagonal particles with uniform morphology having a size around 61 nm. The Brunauer-Emmett-Teller (BET) surface area measurements showed a type III isotherm with calculated surface area of 152 m^2/g. The plot of ln σ_{ac} vs. temperature as a function of frequency indicates a semiconducting behavior with ferroelectric phase transition at 605 K. The calculated activation in the ferroelectric region is 0.93 eV suggests the predominance of hopping conduction mechanism. Kinetic analysis of TG data according to different integral methods showed that in the $NiC_2O_4{\cdot}2H_2O$–TiO_2 precursor, the water molecules are coordinately bounded and the presence of TiO_2 reduces the activation energy needed to the oxalate decomposition reaction.

1. Introduction

The industrial materials titanium based ilmenite-type perovskites with general formula $MTiO_3$ (M = transition metal) have attracted great interest over the past decades because of their utilization in the field of pigments, photoactive catalysts, sensors, and so forth, due to the specially electronic and optical properties as well as the highly chemical stability, large surface areas and non-toxicity [1–4].

Nickel titanate ($NiTiO_3$), being one member of this well-known binary oxides family, has a broad range of the above-mentioned properties and is applicable for industries, such as semiconductor rectifiers [5], electrodes of solid oxide fuel cell [6], metal-air barrier [7], hydrocarbonate catalyzers [8] and gas sensors [9]. $NiTiO_3$ has been also investigated as a tribological coating to reduce friction and wear in high temperature applications without using liquid lubricants [10,11].

The electronic properties of ceramics are greatly affected by the characteristics of the powder, such as

* Corresponding author. Chemistry Department, Faculty of Science, Benha University, Al-Hayaa, Benha, Egypt.
E-mail address: mgabalabdonada@yahoo.com (M.-F. Gabal).

1631-0748/$ – see front matter © 2013 Published by Elsevier Masson SAS on behalf of Académie des sciences.
http://dx.doi.org/10.1016/j.crci.2013.01.009

particle size, morphology, purity and chemical composition. Many efforts have been aimed to improve these properties by controlling their microstructure.

It is still a great challenge to search for a simple and cost-effective route to prepare nano-structured $NiTiO_3$ with a high yield. The traditional solid-state method used in preparing $NiTiO_3$ powder leads to poor homogeneity and high sintering temperatures. At the same time, many methods, such as sol-gel, the flux method, co-precipitations, solid-state reactions, electrospinning and the Pechini process, have been reported for the synthesis of crystalline $NiTiO_3$ powders [12–15].

Phani and Santucci [16] prepared $NiTiO_3$ thin films by sol-gel method using titanium isopropoxide and nickel acetate. Structural, morphological and elemental evolution were characterized by X-ray diffraction (XRD), tapping mode atomic force microscopy and X-ray photoelectron spectroscopy.

$NiTiO_3$ powders were prepared by a simple co-precipitation technique using ammonium carbonate and stoichiometric amounts of $Ni(NO_3)_2$ and $TiOCl_2$ [11]. The phase evolution was investigated by XRD patterns. Particle size and morphology was studied by transmission electron microscopy (TEM).

Nanocrystalline $NiTiO_3$ powders were produced at low temperature of 500 °C by sol-gel route [14]. XRD patterns and Fourier transform infrared (FT-IR) spectroscopy revealed that the powders contained $NiTiO_3$ besides impurities of NiO, as well as anatase and rutile-TiO_2 depending on the annealing temperature and Ni:Ti molar ratio. Based on Brunauer-Emmett-Taylor (BET) analysis, the synthesized powders showed a mesoporous structure containing pores with needle and plate-like shapes.

$NiTiO_3$ microtubes was constructed successfully via a simple solution-combusting method employing a mixture of ethanol and ethyleneglycol, nickel acetate, tetra-*n*-butyl titanate and oxygen gas [12]. The as-obtained product was characterized by XRD patterns, TEM, scanning electron microscopy (SEM), and energy dispersive X-ray spectrometry (EDS). The BET surface area of the product was 14.06 m^2/g and the pore size distribution mainly located from 20 to 30 nm.

Pure $NiTiO_3$ nanopowders were prepared by wet-chemistry method, using nickel stearate, tetra-*n*-butyl titanate and stearic acid [17]. The synthesis process was followed using thermal analysis techniques. FT-IR, XRD and TEM were used to characterize the crystallization process, the particle size and morphology of the calcined powders.

Therefore, in this paper, we communicate two simple processes for preparing nanocrystalline nickel titanate powder. These processes involve the formation of entire titanate through the thermal decomposition reaction of stoichiometric coprecipitated or impregnated mixture of nickel oxalate-dihydrate and titanium dioxide (anatase). The formation process and structural characterization of $NiTiO_3$ will be investigated by DTA-TG, FT-IR, XRD, and TEM. Furthermore, the specific surface area and electrical properties will be also evaluated. In addition, a mechanism for the thermal decomposition process and the kinetic parameters will be achieved using non-isothermal TG curves.

2. Experimental details

2.1. Materials

Nickel nitrate hexahydrate; $Ni(NO_3)_2{\cdot}6H_2O$, basic nickel carbonate; $NiCO_3.2Ni(OH)_2{\cdot}4H_2O$, oxalic acid; $H_2C_2O_4$ and titanium dioxide (anatase); TiO_2 were employed as the starting reagents. All chemicals are of analytical grade (BDH) and used without any further purification.

2.2. Synthesis of $NiTiO_3$ powders

Nickel titanate ($NiTiO_3$) powder were synthesized through the thermal decomposition reaction of $NiC_2O_4{\cdot}2H_2O$–TiO_2 precursor prepared through the impregnation technique or the coprecipitation route.

In the impregnation technique [18], pure $NiC_2O_4{\cdot}2H_2O$ was prepared by direct precipitation, using oxalic acid added dropwise to a solution containing the calculated amounts of nickel nitrate. The obtained fine precipitate was filtered, washed with distilled water and dried. Few drops of bi-distilled water were then added to weighed mixture of both $NiC_2O_4{\cdot}2H_2O$ and TiO_2 (1:1 mole ratio) with vigorous stirring to assure complete homogeneity. The wetted mixture was then dried at 80 °C.

In the co-precipitation method [19], TiO_2 was added to an aqueous solution containing a stoichiometric amount of $NiCO_3{\cdot}2Ni(OH)_2{\cdot}4H_2O$ under vigorous stirring. A stoichiometric amount of oxalic acid solution was then added dropwise into the suspension under constant stirring. During this process, the formed nickel oxalate will be precipitated on the surface of TiO_2 particles by heterogeneous nucleation. The resulting solution was then evaporated until dryness.

Samples of the prepared precursors were then calcined at different temperatures to characterize the decomposition reaction and follow titanate formation. The calcination temperatures and calcination times were 400 °C for 30 min, 600, 800 or 1000 °C for 2 h.

2.3. Characterizations

The decomposition course of the precursors and titanate formation were followed using simultaneous differential thermal analysis-thermogravimetry techniques (DTA-TG). The measurements were carried out using a Perkin–Elmer, STA 6000 thermal analyzer up to 1000 °C at a heating rate of 5 °C/min in air atmosphere. For kinetic measurements, other heating rates of 1, 2 and 3 °C/min were used.

The structure of the powders is examined by X-ray diffraction technique (XRD) using a Bruker D8 high-resolution diffractometer with nickel filtered Cu Kα radiation.

The Fourier transform infrared (FT-IR) spectra of the samples were recorded in the range 4000–200 cm^{-1} on JASCO FT-IR 310 spectrometer using the KBr pellet method.

The transmission electron microscopy (TEMJ) image of the $NiTiO_3$ nanopowders was obtained using an electron microscope (JEOL-2010) operating at 100 kV. The samples were prepared by ultrasonically dispersing the powder in

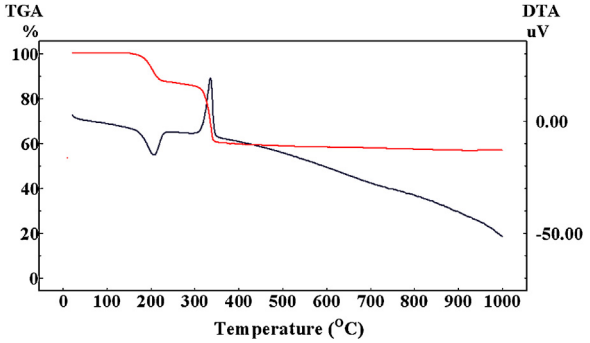

Fig. 1. DTA-TG curves for the thermal decomposition of $NiC_2O_4{\cdot}2H_2O$–TiO_2 precursor in air at heating rate of 5 °C/min.

ethanol and allowing a drop of this to dry on a carbon-coated copper grid.

The Brunauer, Emmett and Teller (BET) method has been used to determine the specific surface area of titanate by means of a nitrogen adsorption isotherm on a Micromeritics, ASAP 2010.

For the electrical measurements, titanate powder was pressed into a pellet under a pressure of 2 ton/cm^2. The polished pellet with a silver paint was used for measuring temperature-dependent electrical conductivity, at different frequencies (100 Hz–5 MHz), using a Hioki LCR bridge model 3531.

3. Results and discussion

3.1. Thermal analysis studies

To investigate the different crystalline intermediates resulting from the thermal decomposition course of coprecipitated $NiC_2O_4{\cdot}2H_2O$–TiO_2 precursor and find out the optimum calcining temperature for titanate formation, the corresponding DTA-TG thermogram was conducted and illustrated in Fig. 1.

From the figure, it is clear that the decomposition proceeds through two weight loss steps in the range 160–360 °C. The observed DTA peaks are closely corresponding to the obtained weight losses. The two steps, based on the decomposition range and weight loss calculations, can be assigned to the decomposition of the oxalate contents of the precursor.

The first step (Obs. Wt loss = 13.6%) is mostly due to dehydration with the loss of two water molecules (Calc. Wt. loss = 13.7%). The endothermic DTA peak characterizing this dehydration lies in the range 163–234 °C with peak temperature at 207 °C. This dehydration range suggests that the water molecules are coordinately bounded to the oxalate moiety [20]. The second TG step (Obs. Wt loss = 27.5%) between 300 and 360 °C seems to be associated with the decomposition of anhydrous nickel oxalate with the formation of NiO. The accompanying exothermic peak at 336 °C can be attributed to the oxidation of Ni metal and CO decomposition products to NiO and CO_2, respectively [21,22].

No excessive weight loss or DTA change can be detected after 360 °C, suggesting the inability of titanate formation within this temperature range.

DTA-TG thermogram of the impregnated $NiC_2O_4{\cdot}2H_2O$–TiO_2 precursor showed consistent behavior with that estimated for coprecipitated precursor.

3.2. X-ray diffraction patterns

XRD patterns taken for the as-prepared precursors as well as their calcined powders at different temperatures are shown in Figs. 2 and 3. From the figures, it is obvious that, the two as-prepared precursors as well as their calcined powders at 400, 600 and 800 °C showed identical XRD patterns.

The as-prepared precursors exhibited XRD peaks, which can be assigned to the tetragonal TiO_2 (anatase) and $NiC_2O_4{\cdot}2H_2O$ (JCPDS file No.: 78-2486 and JCPDS file No.: 14-0742, respectively). XRD of the calcined precursors at

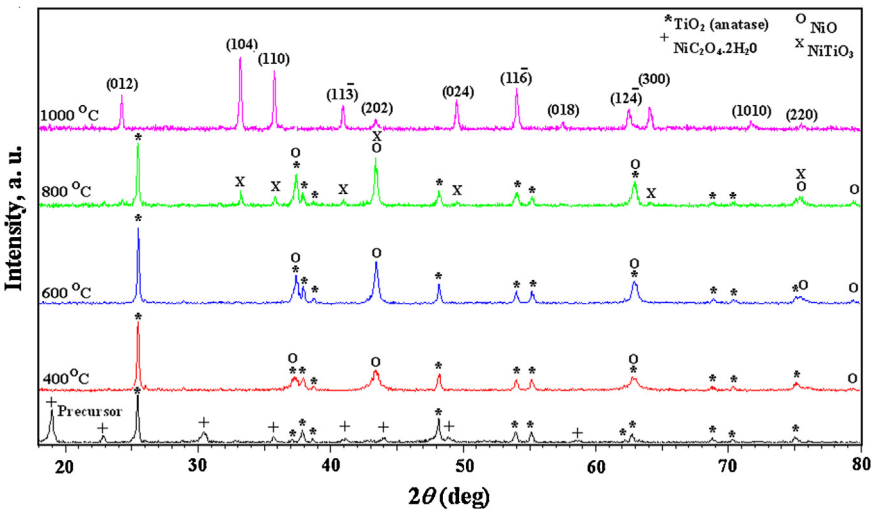

Fig. 2. XRD patterns of impregnated $NiC_2O_4{\cdot}2H_2O$–TiO_2 precursor calcined at different temperatures.

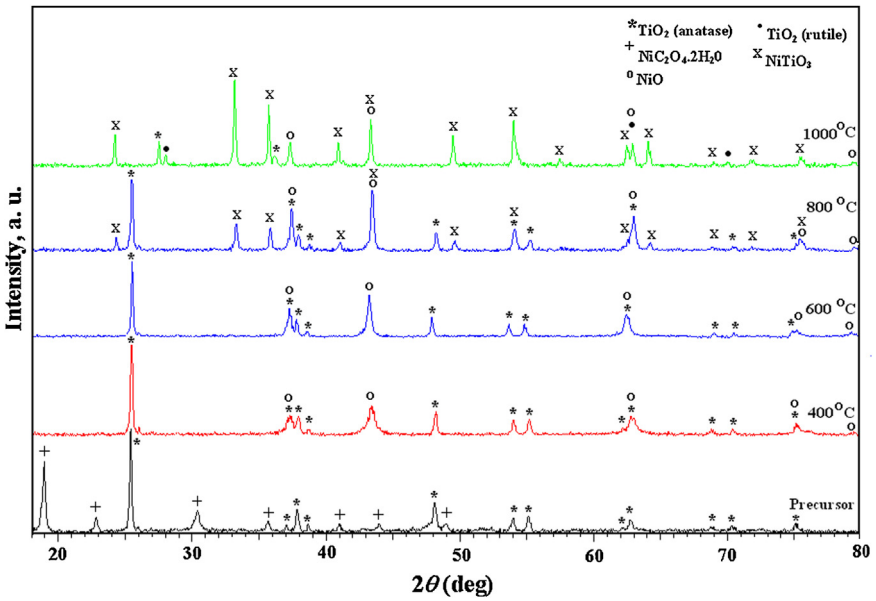

Fig. 3. XRD patterns of coprecipitated $NiC_2O_4{\cdot}2H_2O$–TiO_2 precursor calcined at different temperatures.

400 °C revealed, consistently with DTA-TG measurements, the appearance of the characteristic peaks of NiO (JCPDS file No.: 78-0423) produced from the decomposition of nickel oxalate content besides those of TiO_2 (anatase). No obvious changes are observed by rising the calcination temperature to 600 °C while, at 800 °C, the characteristic XRD peaks of titanate are evidenced; $NiTiO_3$ started to appear besides those assigned to NiO and anatase-TiO_2.

The XRD pattern of the impregnated $NiC_2O_4{\cdot}2H_2O$–TiO_2 precursor calcined at 1000 °C (Fig. 2) showed that all the peaks can be indexed for complete formation of $NiTiO_3$ powders with a single-phase rhombohedral structure and space group of $R\bar{3}$(148) and six formula units per unit cell (JCPDS file No.: 76-0334 or 33-0960). The calculated lattice parameters ($a = b = 5.0252$ Å, $c = 13.7761$ Å) agree well with those reported [11,23]. The average crystalline size calculated from full width half maximum (FWHM) using the Scherrer formula [24] for the reflections in Fig. 2 is found to be 87 nm. The X-ray density calculated using estimated lattice parameters is 4.43 g/cm^3.

On the other hand, XRD patterns of the calcined coprecipitated $NiC_2O_4{\cdot}2H_2O$–TiO_2 precursor at 1000 °C (Fig. 3) exhibits some impurity peaks, which can be indexed to NiO, TiO_2 (anatase) and TiO_2 (rutile) (JCPDS file No.: 82-0514) phases, besides characteristic $NiTiO_3$ peaks. This suggests, in accordance with the reported results in the literature [1,14], the incompletion of the titanate single-phase within this temperature range. The phase transformation of the higher total free energy anatase-TiO_2, at such high temperature, results in the formation of more stable rutile structure [25].

3.3. Morphological study

Fig. 4a shows SEM micrograph of $NiTiO_3$ powder obtained through the impregnation method. The

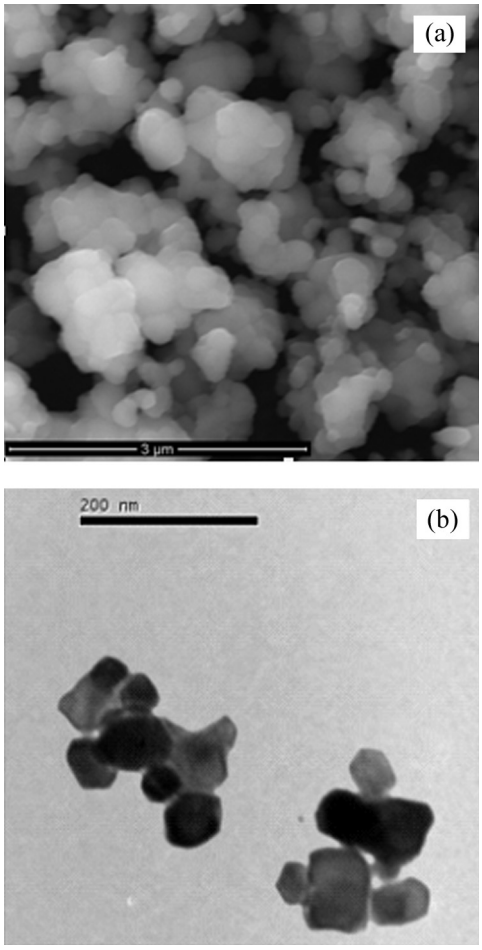

Fig. 4. (a) Low magnification SEM image and (b) TEM image of $NiTiO_3$ powder.

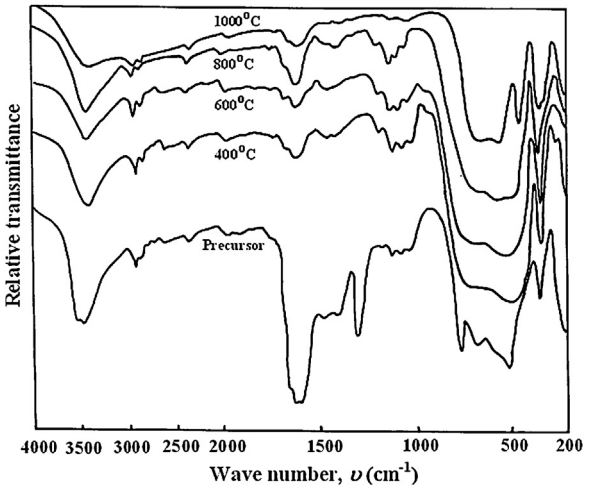

Fig. 5. FT-IR spectra of $NiC_2O_4{\cdot}2H_2O$–TiO_2 precursor calcined at different temperatures.

micrograph reflects the agglomeration nature of the particles with porous morphology. The particles are agglomerated into clusters of varying sizes and shapes. The size of the particles can be identified using TEM technique. TEM image of the powder (Fig. 4b) exhibited hexagonal particles with uniform morphology in size and shape. The average size is around 61 nm, which is slightly smaller than that obtained through XRD patterns.

3.4. FT-IR spectra

Fig. 5 exhibited the FT-IR spectra of the as-prepared impregnated precursor along with its calcined samples at different temperatures. FT-IR spectrum for the as-prepared precursor shows a broad absorption band around 3740 cm^{-1} due to the stretching vibration of O–H group. The absorption band appearing at 1650 cm^{-1} can be assigned to the asymmetric vibrations of the carbonyl group, while the strong band at 1300 cm^{-1} is assigned to the symmetric mode. The bands at 773 and 512 cm^{-1} are attributed to the out-of-plane bending mode of water and O–C–O in-plane bending mode of oxalate, respectively [26]. The band at 352 cm^{-1} can be assigned to the vibration of metal ion, and the bands at 675 and 2929 cm^{-1} to the presence of TiO_2 [27].

The spectrum of the calcined precursor at 400 °C showed a decrease in the intensities of the bands characteristic for the carbonyl group due to the decomposition of the oxalate content with the formation of metal oxides. Consequently, the new broad intense bands appearing at 681 and 525 cm^{-1} can be assigned to the metal-oxygen and TiO_2 vibrations, respectively [19].

Similar spectra are observed for powders calcined at 600 and 800 °C. The appearance of a new band at 566 cm^{-1} in the spectrum of powder calcined at 800 °C indicating, in accordance with XRD patterns, the starting of titanate formation. At 1000 °C, the three characteristic bands observed at 651, 567 and 461 cm^{-1} can correspond to the formation of $NiTiO_3$ powders in accordance with previously reported results [10,14,28].

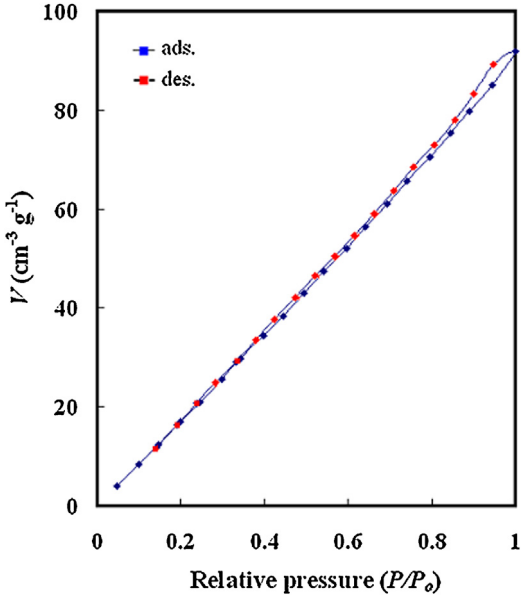

Fig. 6. N_2 adsorption/desorption isotherm obtained for $NiTiO_3$.

3.5. BET measurement

Fig. 6 illustrates the N_2 adsorption-desorption isotherms of impregnated precursor annealed at 1000 °C. The isotherm represents a type III isotherm, which describes adsorption on macroporous adsorbents with weak adsorbate-adsorbent interactions [29]. The specific surface area measured by the BET method (S_{BET}) is 152 m^2/g. This relatively high value compared to those reported in the literature [12,14,23] suggests the validity of the present synthesis route in obtaining nano-sized titanate powder, with very high surface area, having applications in catalysis, separation and purification processes.

3.6. AC conductivity

The plot of conductivity ($\ln \sigma_{ac}$) for $NiTiO_3$ powder as a function of temperature and frequency is illustrated in Fig. 7. The figure indicates that the conductivity shows strong dependence on both temperature and frequency of the applied field. At low temperatures, the conductivity shows a metallic behavior in which the conductivity is nearly stable with increasing temperature. By increasing temperature, a pronounced peak at 605 K is observed after which an obvious increase in the conductivity values with increasing temperature is revealed. The appearance of this peak can be attributed to a ferroelectric phase transition [30,31]. Singh et al. [30] has reported a marked change in the conduction mechanism of $NiTiO_3$ at 700 K during measuring electrical conductivity as a function of temperature. Bamzai et al. [31] indicated, through measuring the dependence of dielectric constant, dielectric loss and AC conductivity on applied frequency and temperature, the appearance of this peak at 773 K instead of 700 K.

The increase in the conductivity at high temperatures can be explained by considering the mobility of charge

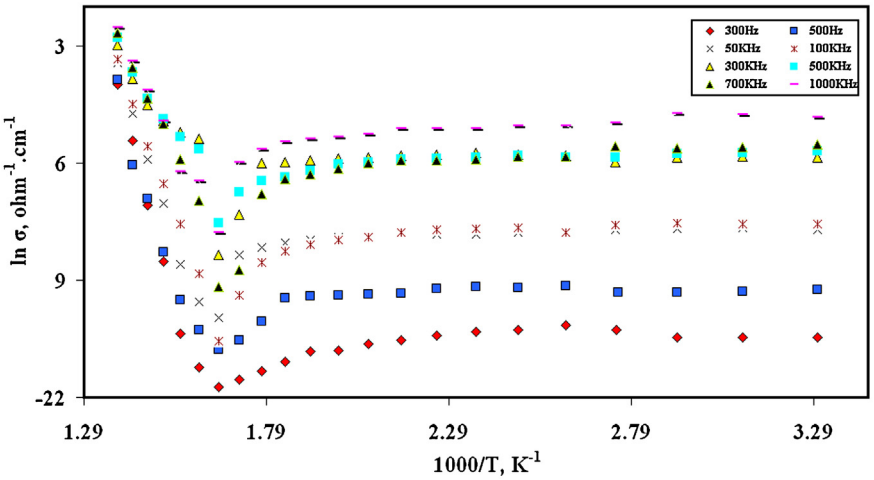

Fig. 7. Relation between ln σ_{ac} and the reciprocal of the absolute temperature as a function of applied frequency for $NiTiO_3$.

carriers responsible for hopping which increases also by increasing temperature. This situation suggests semiconducting behavior of $NiTiO_3$. The activation energy per mole (E_a) required for this hopping process, calculated in the ferroelectric region from the slope of ln σ_{ac} versus reciprocal of absolute temperature, is 0.93 eV. This higher value than 0.2 eV per molecule suggests that the conduction mechanism is due to hopping [30].

The obvious increasing of AC conductivity with increasing frequency is a characteristic feature of materials where hopping mechanism dominates [31].

3.7. Kinetic studies

To characterize the solid-state decompositions mechanism during thermal treatment of $NiC_2O_4{\cdot}2H_2O$–TiO_2 precursor, aiming at the production of $NiTiO_3$, the kinetic analysis under non-isothermal conditions of TG curves was carried out using different heating rates and assuming different solid-state reaction equations [20] The kinetic parameters: E, activation energy (kJ/mol) and A, frequency factor (min^{-1}) were calculated in view of three integral methods: Diefallah's composite method [20,32,33], Coats–Redfern method [34] and Ozawa method [35]. The details of these methods were reported elsewhere [20,32].

The composite method involves a model-fitting kinetic approach, since it does not assume a particular reaction model, but it allows the choice of the kinetic mechanism which best fits the data and gives the highest correlation coefficient [32]. Fig. 8 correlates representative weight changes as a function of temperature obtained from non-isothermal measurements. Kinetic analysis according to the composite method assuming different models of heterogeneous solid-state reactions (Table 1) shows that the dehydration step is best described by phase boundary controlled reaction mechanism (R_2 and R_3), in which the reaction is controlled by the movement of an interface at constant velocity and nucleation occurs virtually instantaneously. On the other hand, the oxalate decomposition step follows

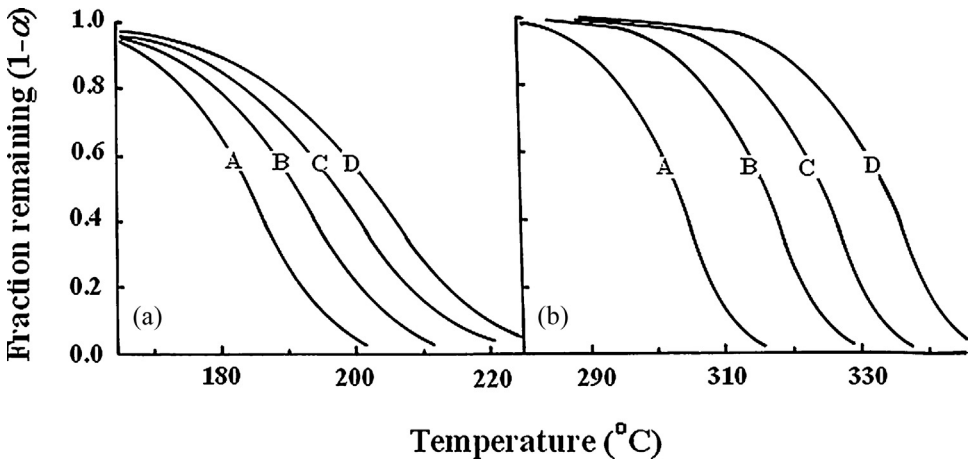

Fig. 8. Non-isothermal measurements for the thermal decomposition in air of $NiC_2O_4{\cdot}2H_2O$–TiO_2 precursor: (a) dehydration and (b) decomposition of oxalate content Heating rate: curve A, 1 °C/min; curve B, 2 °C/min; curve C, 3 °C/min and curve D, 5 °C/min.

Table 1
Activation parameters for non-isothermal decomposition in air of the $NiC_2O_4{\cdot}2H_2O$–TiO_2 precursor, calculated according to the composite method, assuming different kinetic models.

Model	Dehydration (step I)			Decomposition (step II)		
	E (kJ/mol)	log A (min^{-1})	r	E (kJ/mol)	log A (min^{-1})	r
D_1	200 ± 4	21.1 ± 0.5	0.981	382 ± 33	32.4 ± 3.1	0.817
D_2	217 ± 4	22.8 ± 0.5	0.982	403 ± 35	34.2 ± 3.3	0.813
D_3	238 ± 4	24.7 ± 0.5	0.982	431 ± 39	36.2 ± 3.6	0.807
D_4	224 ± 4	23.0 ± 0.5	0.982	413 ± 36	34.4 ± 3.4	0.811
R_2	123 ± 2	12.4 ± 0.2	0.987	246 ± 13	20.4 ± 1.2	0.914
R_3	128 ± 2	12.9 ± 0.2	0.990	253 ± 14	20.8 ± 1.3	0.910
F_1	140 ± 2	14.7 ± 0.2	0.993	268 ± 16	22.8 ± 1.5	0.899
F_2	91 ± 5	9.9 ± 0.6	0.877	172 ± 11	14.8 ± 1.0	0.891
F_3	164 ± 8	18.6 ± 0.9	0.908	270 ± 25	24.0 ± 2.4	0.795
A_2	79 ± 4	8.0 ± 0.4	0.917	171 ± 3	14.2 ± 0.3	0.989
A_3	59 ± 4	5.8 ± 0.5	0.811	139 ± 2	11.3 ± 0.2	0.991
A_4	49 ± 5	4.7 ± 0.6	0.723	123 ± 4	9.9 ± 0.4	0.963
E_1	90 ± 11	13.9 ± 1.3	0.642	80 ± 32	9.3 ± 3.0	0.290

Table 2
Activation parameters calculated using different methods for the non-isothermal decomposition in air of $NiC_2O_4{\cdot}2H_2O$–TiO_2 precursor.

Method of analysis	Dehydration (R_3 model)		Decomposition (A_3 model)	
	E (kJ/mol)	log A (min^{-1})	E (kJ/mol)	log A (min^{-1})
Composite	128 ± 2	12.9 ± 0.2	139 ± 2	11.3 ± 0.2
Coats–Redfern	130 ± 19	13.1 ± 0.4	125 ± 10	11.1 ± 0.3
Ozawa	153 ± 23	13.4 ± 0.5	147 ± 4	11.5 ± 0.3

Avrami–Erofeev random nucleation mechanism (A_2, A_3 and A_4) characteristic for random nucleation growth. The other reaction models gave less satisfactory results.

The activation parameters were then also calculated using Coats–Redfern and Ozawa methods assuming R_3 and A_3 models for the dehydration and oxalate decomposition steps, respectively. The calculation results according to the three methods are summarized in Table 2. The results show a good agreement (within the experimental errors) between the values of the calculated activation parameters assuming different calculation methods.

It is well known that the activation energy for the losing of crystal water lie in the range 60–80 kJ/mol, while the value for the coordinately bounded one are within the range 130–160 kJ/mol [20]. The obtained activation energy for the oxalate dehydration (Table 2) suggests that the water molecules are coordinately linked water. This result agrees well with the dehydration temperature obtained from DTA-TG experiments.

The obtained activation energy for the oxalate decomposition reaction (Table 2) appears to be lower than that reported in the literature [22,36]. This can be attributed to the presence of titanium dioxide during the thermal decomposition of oxalate, which can act as a spacer causing fewer points of contact between particles of nickel oxalate and increasing the interfaces, which facilitates the decomposition and consequently, decreases the activation energy.

4. Conclusions

In summary, single-phase $NiTiO_3$ nanopowders was successfully synthesized through simple impregnation technique using the $NiC_2O_4{\cdot}2H_2O$–TiO_2 precursor. The thermal decomposition course of precursor was followed by DTA-TG measurements. Calcined samples of precursor at different temperatures were investigated using XRD patterns and FT-IR spectra to evaluate the formation of $NiTiO_3$ phase. Particle size and morphology of $NiTiO_3$ nanopowders studied by TEM image revealed the presence of hexagonal nano-particles with a size of 61 nm. BET measurements estimated a very large surface area of 152 m^2/g suggesting its use as a catalyst. AC conductivity measurements as a function of temperature revealed a semiconducting behavior with the predominance of a hopping conduction mechanism. In addition, the obtained ferroelectric phase transition at 605 K suggests ferroelectric properties at such high temperature range. Kinetic analysis of the non-isothermal TG curves showed that the presence of TiO_2 reduces the activation energy for the oxalate decomposition.

Acknowledgement

This paper was funded by the Deanship of Scientific Research (DSR), King Abdulaziz University, Jeddah, under grant No. [518-130-1432]). The authors therefore acknowledge with thanks DSR technical and financial support.

References

[1] J. Jiang, Q. Gao, Z. Chen, J. Hu, C. Wu, Mater. Lett. 60 (2006) 3803.
[2] Y. Zhang, S.G. Ebbinghaus, A. Weidenkaff, T. Kurz, H.A.K. Nidda, P.J. Klar, M. Gungerich, A. Reller, Chem. Mater. 15 (2003) 4028.
[3] F. Guifen, S.V. Patricia, L. Chhiu-Tsu, J. Phys. Chem. B 109 (2005) 8889.

[4] J.H. Yang, J.D. Henao, M.C. Raphulu, Y.M. Wang, T. Caputo, A.J. Groszek, M.C. Kung, M.S. Scurrell, J.T. Miller, H.H. Kung, J. Phys. Chem. B 109 (2005) 10319.
[5] H. Wendt, G. Imarisio, J. Appl. Electrochem. 18 (1988) 1.
[6] O. Yamamoto, Y. Takeda, R. Kanno, M. Noda, Solid State Ionics 22 (1987) 241.
[7] Y. Shimizu, K. Uemura, N. Miura, N. Yamzoe, Chem. Lett. 67 (1988) 1979.
[8] M. Skoglundh, L. Lowedalh, K. Janson, L. Dahl, M. Nygren, Appl. Catal. 53 (1970) 56.
[9] H. Obayashi, Y. Sakurai, T. Gejo, J. Solid State Chem. 17 (1976) 299.
[10] N. Dharmaraj, H.C. Park, C.K. Kim, H.Y. Kim, D.R. Lee, Mater. Chem. Phys. 87 (2004) 5.
[11] A.V. Murugan, V. Samuel, S.C. Navale, V. Ravi, Mater. Lett. 60 (2006) 1791.
[12] Y. Ni, X. Wang, J. Hong, Mater. Res. Bull. 44 (2009) 1797.
[13] K.P. Lopes, L.S. Cavalcante, A.Z. Simões, R.F. Gonçalves, M.T. Escote, J.A. Varela, E. Longo, E.R. Leite, J. Sol-Gel Sci. Technol. 45 (2008) 151.
[14] M.R. Mohammadi, D.J. Fray, Solid State Sci. 12 (2010) 1629.
[15] J. Wang, Y. Li, Y. Byon, S. Mei, G. Zhang, Powder Techn. 235 (2013) 303.
[16] A.R. Phani, S. Santucci, Thin Solid Films 396 (2001) 1.
[17] M.S. Sadjadi, K. Zare, S. Khanahmadzadeh, M. Enhessari, Mater. Lett. 62 (2008) 3679.
[18] M.A. Gabal, Y.M. Al Angari, Mater. Chem. Phys. 115 (2009) 578.
[19] M.A. Gabal, Ind. Eng. Chem. Res. 50 (2011) 13771.
[20] El-H.M. Diefalla, Thermochim. Acta 202 (1992) 1.
[21] D. Dollimore, Thermochim. Acta 117 (1987) 331.
[22] A. Coetzee, M.E. Brown, D.J. Eve, C.A. Strydom, J. Therm. Anal. 4 (1994) 357.
[23] K.P. Lopes, L.S. Cavalcante, A.Z. Simoes, J.A. Varela, E. Longo, E.R. Leite, J. Alloys Compds. 468 (2009) 327.
[24] B.D. Cullity, Elements of X-ray Diffraction, second ed., Addison-Wesley, Reading, MA, 1978.
[25] P. Ha, H. Youn, H. Jung, K. Hong, Y. Park, K. Ko, 223, J. Colloid Interface Sci. (2000) 16.
[26] J.M. Ouyang, H. Zheng, S.P. Deng, J. Cryst. Growth 293 (2006) 118.
[27] R.A. Nyquist, R.O. Kagel, The handbook of infrared and Raman spectra of inorganic compounds and organic salts, Academic Press, San Diego, 1997.
[28] Y.J. Lin, Y.H. Chang, W.D. Yang, B.S. Tsai, J. Non-Crystalline Solids 352 (2006) 789.
[29] International Union of Pure, Applied Chemistry, IUPAC, Pure Appl. Chem. 57 (1985).
[30] R.S. Singh, T.H. Ansari, R.A. Singh, B.M. Wanklyn, J. Mater. Chem. Phys. 40 (1995) 173.
[31] K.K. Bamzai, V. Gupta, P.N. Kotru, B.M. Wanklyn, Ferroelectrics 413 (2011) 328.
[32] M.A. Gabal, J. Phys. Chem. Sol. 68 (2007) 1610.
[33] M.A. Gabal, J. Phys. Chem. Sol. 64 (2003) 1375.
[34] A.W. Coats, J.P. Redfern, Nature 20 (1964) 68.
[35] T. Ozawa, J. Therm. Anal. 2 (1970) 301.
[36] T. Palanismy, J. Gopalakrishnan, B. Viswanthan, V. Srinivasan, V.C. Sastri, Thermochim. Acta 2 (1971) 265.